JOURNAL OF MATERIALS SCIENCE 27 (1992) 4829–4841

Review
Plasticity and mass-transfer in contacting nanoparticles

V. G. GRYAZNOV
Institute for High Pressure Physics, RAS, 142092 Troitsk, Moscow Region, Russia
M. Yu. TANAKOV, L. I. TRUSOV
Scientific-Research Enterprise "ULTRAM", Krasnoproletarskaya 32, 103030 Moscow, Russia

The atomic structure of interparticle contact interfaces which present a new type of interface, is reviewed. Such interfaces show long-range elastic stress fields and a marked tendency to reconstruct themselves into more equilibrium structures similar to conventional grain boundaries. The methods of reconstruction (ageing) of the interfaces are analysed in detail. The elastically stressed state in the volume of nanoparticles which have few contacts with neighbouring particles in the ensemble, is investigated. Plasticity and mass-transfer processes leading to the relaxation of these contact stresses are considered. The mechanisms of generation of dislocations and critical pressures of compaction are discussed in detail. Stress-stimulated diffusion initiated by contact pressures is compared with the traditional mass-transfer caused by surface tension during the sintering of conventional coarse-grained powders.

1. Introduction

Studies of the structure and properties of interfaces in polycrystals, thin epitaxial and island films have a rather long history (see, for example, [1–3]) and principal aspects of this matter have been reported in detail.

From the fundamental viewpoint, the compaction of nanopowders in order to obtain "massive" nanocrystals is a very interesting phenomenon, owing to the unusual types of interfaces these ensembles may incorporate. These contact interfaces are substantially less stable than the traditional ones, and tend to decay due to long-range elastic fields generated by the contacts. This review discusses the simplest approaches to the description of the contact interface structure, elastic fields, channels of contact stress relaxation and other related phenomena taking place in the vicinity of a contact.

2. Formation of contact interfaces

Nanoparticles are the objects of very high adhesiveness [4–6]. Because of the strong adhesive forces, the nanoparticle-free surface tends to decrease via the formation of contacts (the interfacial energy is always less than the surface energy) of radius α given by [7]

$$\alpha = l[4.5\pi (1 - \nu) \gamma_d/Gl]^{1/3} \quad (1)$$

where γ_d is the Dupré energy, $\gamma_d = 2\bar{\gamma} - \gamma_I$ where $\bar{\gamma}$ and γ_I are the surface and interface energies, respectively. In this estimate all the contiguous spherical particles are assumed to possess the same radius, l, and elastic moduli, G, ν. From Fig. 1 the radius, α, of contact between originally spherical nanoparticles may be seen to reach relatively large values up to tens of per cent of the nanoparticle radius, l, under the action of surface tension. Certainly, the contact area enlarges with time on account of the surface diffusion which cannot be disregarded, even for rather low homologous temperatures, because diffusion paths in the contacts between nano-objects are very short. On the basis of this strong adhesion, the aggregates of nanoparticles may resist appreciable external loads. This is equivalent to the non-zero effective Young's modulus, E_e [8]

$$E_e \approx \theta\phi^4[G^2\gamma_d/l (1 + \nu)^2]^{1/3} \quad (2)$$

where the numerical factor θ is about 8.5, and ϕ is the green density. The green density in nanopowders is, as a rule, about 0.4–0.6. (Anomalously low green densities of the order of 0.05 may be obtained under certain conditions of nanoparticle production [9].) The substitution of typical values into this relationship gives a rather high effective modulus $E_e \sim 10^{-2} G$. In reality the nanoparticle ensemble changes its density at smaller external loads due to interparticle sliding associated, particularly, with plastic processes in contacts. (The effect of the nanopowder dead weight is, to some extent, equivalent to the external load [9].)

Simple geometric considerations (see Fig. 1) show that a contact perceives external load, $\sigma^{(e)}$, amplified by the factor of $(1/\alpha)^2$. The critical shear stress causing irreversible changes in contacts between nanoparticles may be estimated, if one assumes that the interfacial

0022–2461

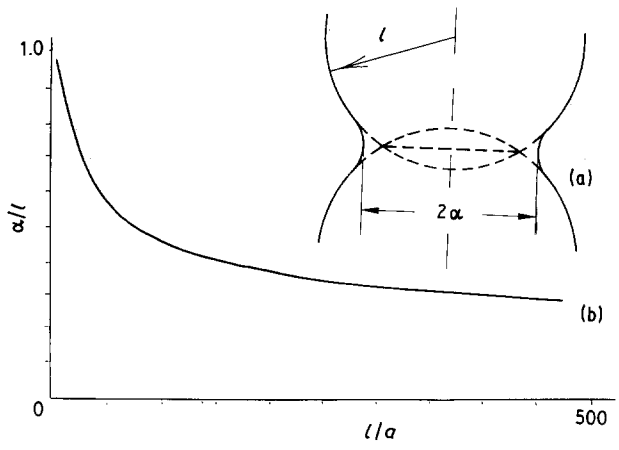

Figure 1 Capillary contact between nanoparticles. (a) Schematic model. (b) Contact radius, α, as a function of nanoparticle radius, l (in terms of lattice parameter, a) for elastic shear modulus $G = 10^{11}\,\mathrm{J\,m^{-3}}$, Poisson's ratio $\nu = 0.3$ and the Dupré energy, $\gamma_d = 6\,10^{-1}\,\mathrm{J\,m^{-2}}$ (gain in surface energy due to formation of contact).

plastic processes become irreversible, when the radius of the bending of the leading glissile dislocation under the action of the local stress $\sigma_{loc} \sim N\sigma^{(e)}\,(1/\alpha)^2$ (where N is the number of dislocations in the contact–interface pile-up) becomes comparable with the radius, α, of the contact. So, stress σ_{loc} should be $\sim Gb/4\alpha$ [10], where $\boldsymbol{b}$ is the Burgers vector of the interface dislocation (the absolute values of the Burgers vectors for interface dislocations are, as a rule, less than those for the lattice ones). Thus, one obtains

$$\sigma_c = \frac{\theta_1}{N} G \left(\frac{\boldsymbol{b}}{l}\right)^{4/3} \left(\frac{\gamma_d}{G\boldsymbol{b}}\right)^{1/3} \quad (3)$$

where coefficient $\theta_1 \approx 0.25\ [4.5\pi(1-\nu)]^{1/3}$. This estimate shows that for nanoparticles of radius $l \sim 10^1\boldsymbol{b}$ (in which case the contact interface contains only a few dislocations, i.e. $N \sim 1$–10) the critical shear stress may be as large as $\sim 10^{-3}\,G$. This rather high value indicates that the interparticle sliding in nanopowders (especially for the aged contacts, i.e. for the contacts with a relaxed structure) is difficult to initiate. If the lattices of contacting nanoparticles fit poorly, the mechanism of interparticle sliding is of a different nature [9, 11].

In addition, the stability of "capillary" (due to surface tension) contacts with respect to the rupture of contacting nanoparticles increases the capacity of nanoparticle ensembles to resist irreversible deformation. The critical stress of the capillary contact rupture, σ'_c, is, in fact, proportional to γ_d/l, which for the nanocrystallite size $l \sim 10^1\boldsymbol{b}$ yields the upper-margin value $\sim 10^{-3}\,G$.

Equations 2 and 3 demonstrate the size-dependent resistance of free nanopowders to external forces. One should note that due to the well-known inclination of nanoparticles to form clusters containing thousands of particles (the average cluster size depends on the prehistory of a nanopowder specimen), the nanopowders may behave like traditional coarse powders. In the latter case the equations mentioned above do not hold.

Compaction of nanopowders requires the application of very high pressures [12, 13]. Under such pressures the local contact stresses may be more important than the adhesion effects. According to the Hertzian theory [14] the component of the stress tensor normal to the contact area obeys the following law

$$\sigma_n = \frac{3}{2}(l/\alpha_H)^2 P(1 - r^2/\alpha_H^2)^{1/2} \quad (4)$$

where P is the external pressure and r the radius in the polar coordinate system with the origin anchored at the contact centre. The expression for the Hertzian contact radius, α_H, takes the form [14]

$$\alpha_H = l\theta_2(P/G)^{1/3} \quad (5)$$

where the numerical factor $\theta_2 = [3\pi(1-\nu)/8]^{1/3}$. Using Equations 4 and 5 one may obtain the maximum pressure over the contact. This maximum value is achieved at the contact centre

$$P_{max} = \theta_3 G(P/G)^{1/3} \quad (6)$$

where the numerical factor $\theta_3 = 1.5\ [3\pi(1-\nu)/8]^{-2/3}$.

For very high external pressures ($P \sim 10^{-2}\,G$) contact stresses could reach huge values ($\sim G$), provided Equations 4–6, derived in the framework of the linear elasticity theory, remain valid. However, as will be shown in Section 4, such high local stresses are not attainable in practice due to the defects generated in the contacts and spreading afterwards from the contact regions.

Shape irregularities, impurity atoms, etc. give rise to friction between nanoparticles. The friction and surface tension account to a considerable degree for the gradients of residual stresses existing in poorly compacted powders at the macroscopic scale to prevent unloading the contacts in an as-compacted sample. However, an allowance for friction forces in the Hertzian problem of normal loadings (without tensile components) gives only non-essential corrections to the present results [15].

Summing up the discussion of this section one should note that in the absence of relaxation processes, high local stresses may exist in contact interfaces either under external load or in the case of pronounced surface-tension effects (the latter situation usually corresponds to small sizes, l, of particles with clean surfaces, see Equation 1). As soon as relaxation phenomena become involved, the considered contact interfaces turn into traditional ones.

3. Structure of contact interfaces

3.1. Structure of defects in unrelaxed contact interfaces

As a rule, nanoparticles are convex, except dendrites and polyparticles (e.g. "dumb-bells" or clusters) which are beyond the scope of the present consideration. They are usually predisposed towards faceting (see, for example, [16, 17]). Therefore, a particle with bcc structure may be represented by a cubic octahedron (Fig. 2). However, the surface ledges are still present even for near-spherical nanoparticles [17, 18].

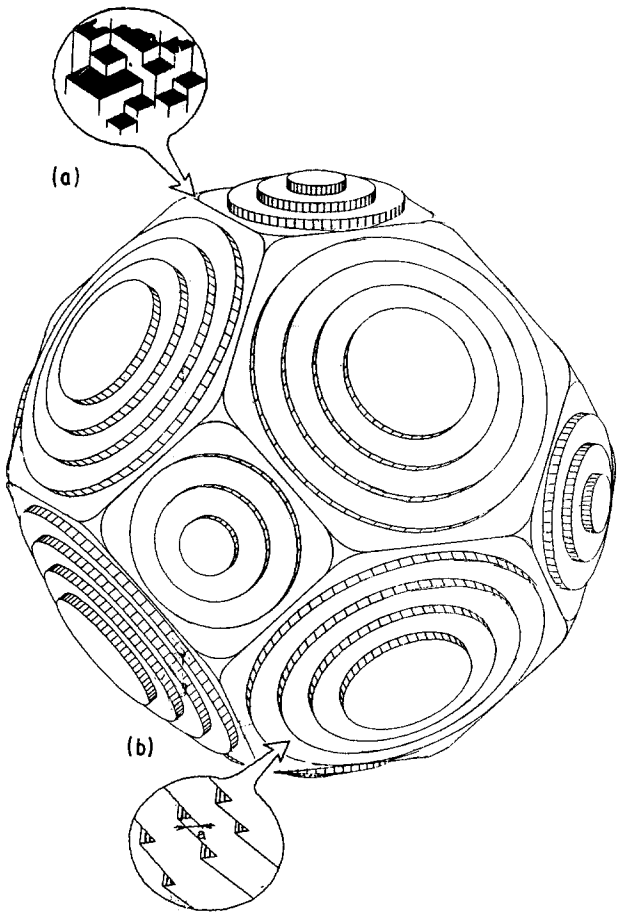

Figure 2 Schematic models of a nanoparticle with b c c lattice structure. (a) Vertex fine structure. (b) Edge fine structure.

Each element of the nanoparticle surface is characterized by its own curvature, the facet curvature radius being R_f, and the rounding-off radii of edges and vertices, R_e and R_v, respectively. For ensembles of near-spherical nanoparticles these radii are typically close to the particle radius, l. Simple geometric considerations show that the average number of ledges on the facet of a nanoparticle with b c c structure is of the order of $(l/a')\ [1 - \cos(\pi/6)]$, where a' is the ledge height (of the order of the lattice parameter, a). For $l \sim 10^2$ nm, a' ~ 0.3 nm, the average number of ledges on the nanoparticle facet is of the order of 50.

The average distance, D, between the ledges comprises about several lattice parameters, a. However, it is not constant but continuously varies along the facet. Its maximum is situated near the centre of the facet, the value at maximum D_0 being approximately 1.4 $(al)^{1/2}$. In this particular case, $D = 3$ nm. D decreases towards the periphery as $D_n \sim (al)^{1/2}\ ((n+1)^{1/2} - n^{1/2})$, where n is the ledge number, counted from the centre of the facet.

Near the rounded vertices, the surface asperity looks like a set of faceted bulges (Fig. 2, inset a), while near the edges it may be represented by a family of approximately parallel ledges (Fig. 2, inset b). The superposition of these ledges in the Hertzian contact area depends on the contacting faces of nanoparticles (Fig. 3).

Fig. 3a illustrates the most probable situation, when two facets are stuck together during the formation of the Hertzian contact. Other situations are less plausible because of inevitable rotations of nanoparticles during compaction. However, if the configurations presented in Fig. 3b and c are stabilized, the ledges and vertices become potential sources of linear and point defects in the contact.

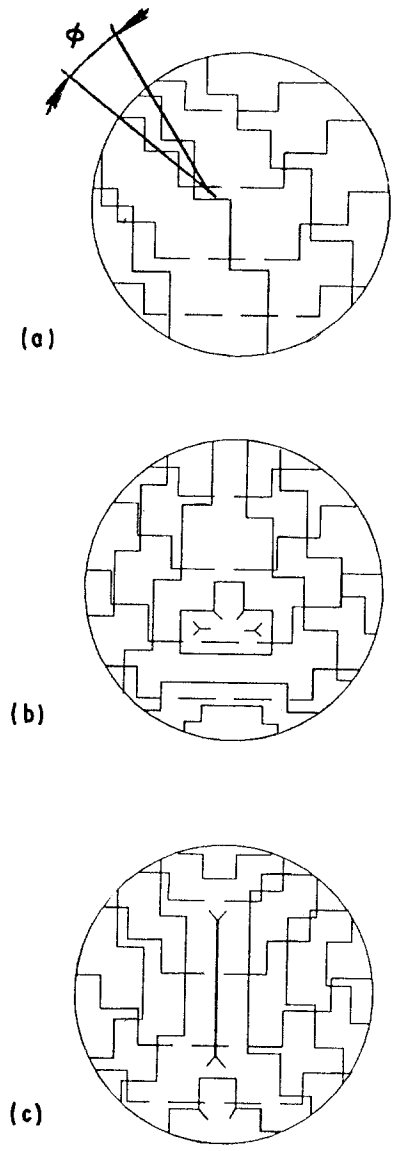

Figure 3 Different types of Hertzian contacts: (– – –) ledges on the surface of the opposing particle. (a) Overlap of facets; φ is the angle between overlapping sets of ledges. (b) Vertex–facet contact. (c) Edge–facet contact.

When nanoparticles come into contact with each other, their surface defects become the contact area internal defects [19]. The surface ledges of particles in the contact area turn into interface dislocations (Fig. 4). The properties of these dislocations coincide with the properties of typical interface dislocations. The only peculiarity of such dislocations in the situation being considered, is that they form unstable configurations that should either relax or disappear after unloading.

The configurations shown in Fig. 3a may form a dislocation network with the typical segment length $\mathscr{D} \sim D_n/\sin\varphi$, where φ is the angle between the two sets of interacting ledges.

A similar situation is shown in Fig. 4 which illustrates the process of forming the edge interface dislocations. Networks of screw interface dislocations

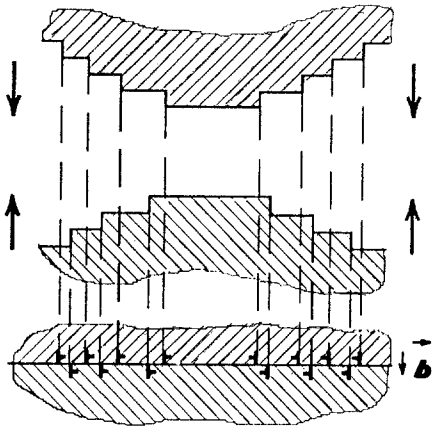

Figure 4 Model of the formation of interface dislocation by ledges on contacting facets of nanoparticles.

may, for example, be formed due to misorientations of crystal lattices of contacting nanoparticles.

If the edge of a nanoparticle is set against the facet of another nanoparticle in one of the contacts, a wedge interface disclination may be created in the contact area (Fig. 5). The coordination number for nanoparticles in nanopowders with a high green density, ϕ, is of the order of 10, and the probability of this event becomes appreciable for each nanoparticle of the ensemble. If diffusion and plastic processes in the interface are suppressed, these interface disclinations may exist in compacts.

Interface disclinations can produce long-range elastic stresses in nanoparticles [20]

$$\sigma_{loc} \sim \frac{G\omega}{2\pi(1-\nu)} \log(\theta l/\alpha_H) \qquad (7)$$

where the disclination power, ω, depends on the value of angle β (Fig. 5) and the numerical factor, θ, may be estimated as $\sim 10^{-1}$. These interface disclinations may seriously modify the Hall–Petch law.

3.2. Fine structure of relaxed contact interfaces

Relaxation processes in contact interfaces result in the disappearance of long-range elastic fields and in the change of interface structure (Fig. 6). Owing to the surface diffusion, the radius of the diffusion (or adhesion [7], see Fig. 1) neck increases with time and may become comparable with the nanoparticle radius, if the temperature conditions allow diffusion processes to develop [21, 22] (Fig. 6a).

Interface long-range elastic fields may relax due to faceting of the interface via the migration of some segments of the contact interface [23] (Fig. 6b). The contact–interface migration may be accompanied by the rotation of contacting nanoparticles. It is worth mentioning that the interface previously distorted may be transformed due to the migration into a faceted interface consisting of segments with special orientations (coinciding-site lattice (CSL)-boundaries; see, for example [24]).

Generally speaking, the effective elastic moduli of contacting nanoparticles may differ. This is the case for the mixtures of nanopowders and for the nanoparticles with anisotropic elastic properties. So, the contact interface may bend into a particle having lower effective elastic moduli (Fig. 6c). Such an interface when relaxing is capable of nucleating a new one. It is interesting to note that convex interfaces have been recently detected in as-compacted nanocrystals [25]. It is thought that the nucleation of additional interfaces (primary recrystallization) near the contacts contaminated with impurity atoms is hindered.

The non-equidistant positions of dislocations in pile-ups are well-known to generate highly intensive elastic fields near the pile-up head [10]. Therefore, the energy of the dislocation structure which inherits the geometry of facet ledges (see Fig. 3) may be decreased at the expense of a more regular arrangement of the interface dislocations [26, 27] (Fig. 6d). Such a structure of dislocations possessing low energy shows localized stress fields. Tholen [26] has noted that in spite of the proximity to the surface, such relaxed interfaces look like typical polycrystal ones.

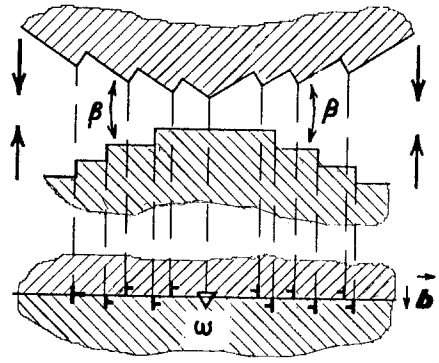

Figure 5 Origination of a wedge interface disclination from a nanoparticle edge.

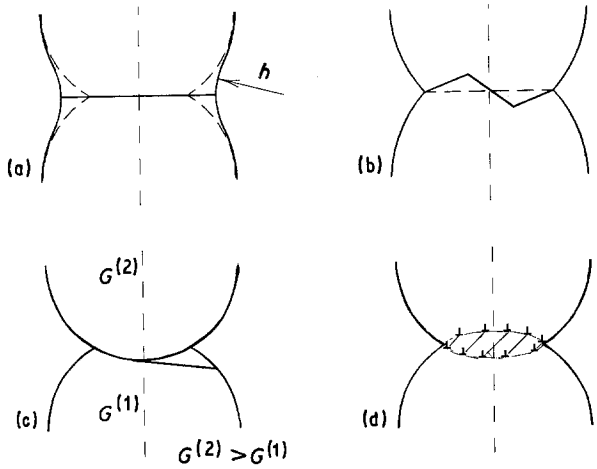

Figure 6 Structure of relaxed contact interfaces. (a) Growth of diffusion neck as a result of initiation of surface diffusion. (– – –) The original position of the nanoparticle surface. (b) Faceting the interface as a result of local migration. (– – –) The initial position of the contact interface. (c) Nucleation of a new grain boundary at a convex contact interface. (——) New boundary. (d) Equidistant interface dislocations.

4. Elastic stress fields inside nanoparticles in loaded nanopowders

The plastic and diffusion processes in nanoparticles which develop in nanopowders when compacted are

closely linked with the local elastic stresses generated during the formation of elastic contacts between the neighbouring nanoparticles. The details of the contact stress distribution should substantially influence both plastic and diffusion processes as well as the final characteristics of as-compacted nanocrystals.

Contact problems have been studied for a long while (see [28]). However, the distributions of all the elastic field components in the whole volume of an elastic sphere having several Hertzian contacts with equivalent spheres, have not been evaluated until quite recently [29].

This problem is discussed in the present section (after Tanakov *et al.* [29]), where the three-dimensional finite element method has been adopted for the analysis which has been carried out, with the following typical assumptions.

1. Nanoparticles are perfect homogeneous isotropic elastic spheres.

2. All the nanoparticles in the ensemble are identical and contain only Hertzian contacts; in addition, nanoparticles are supposed to be packed in regular structures.

3. Any imperfections are absent from the contacts and the temperature is low enough to initiate the sintering processes (the opposite case has been discussed, e.g. [30]).

4. Sizes, l, of nanoparticles are less than the critical length, l^*, of dislocation stability [31] or else the stress relaxation processes make the applicability of the Hertzian approach doubtful [32].

It is interesting to study three typical cases of the loadings of nanoparticles in ensembles (Fig. 7). For symmetry reasons, the calculations have been restricted to only one quadrant of the sphere.

In a nanoparticle compressed by neighbours the most informative quantities are hydrostatic and tensile components of elastic stress fields. Calculations have been performed for three contact radii: $\alpha_H = 0.05\ l$, $0.1\ l$ and $0.15\ l$. In the two-contact model (Fig. 7a) they correspond to the following values of the external pressure $P_{two} = 1.5 \times 10^{-4}\ G$, $1.2 \times 10^{-3}\ G$, $4.1 \times 10^{-3}\ G$. For a nanoparticle having eight contacts, one obtains $P_{eight} = 3.5 \times 10^{-4}\ G$, $2.8 \times 10^{-3}\ G$, $9.6 \times 10^{-3}\ G$, while for twelve contacts $P_{twelve} = 4.2 \times 10^{-4}\ G$, $3.4 \times 10^{-3}\ G$, $1.2 \times 10^{-2}\ G$, respectively (see Table I). The last model, when applied to a tungsten nanopowder yields effective pressures $P_{twelve} = 0.06$, 0.5, 1.9 GPa. These pressures are not very high, but they may induce substantially higher local stresses near the contacts.

4.1. A two-contact model (Fig. 7a)

For real nanopowders with high green densities, such a small number of neighbours is rather exotic. Nevertheless, this model illustrates the basic features of elastic fields in a loaded nanoparticle and permits useful approximations to be obtained describing the properties of the stressed state in nanoparticles.

The distributions of the hydrostatic stress and the intensity of tensile stresses are represented in Fig. 8. An accurate analysis of numerical data has revealed an increase in the inhomogeneity of the elastic fields with the external pressure rise. However, the slight dependence of the volume of the dilated region, which is, in this case, nearly 6%, on the external pressure, is surprising.

The tensile stresses in the central part of the sphere grow with the external pressure increase. A careful examination of the numerical data has shown the presence of a slightly pronounced maximum of shear stresses right under the Hertzian contact at $\alpha_H = 0.15\ l$. This typical peak [28] has not been resolved in other cases, because of an unavoidable averaging procedure smoothing the local non-monotonies.

The numerical data for the hydrostatic stress, $p(r, z)$, and the intensity of the shear stresses, $\tau(r, z)$, inside a loaded nanoparticle in the case of two Hertzian contacts may be approximated by rather simple Equations

$$p(r, z) = \frac{0.5}{0.003 + (r/l)^{1.6} + (z/l)^{1.8}} P \quad P < 0 \qquad (8)$$

and

$$\tau(r, z) = \frac{2}{0.003 + (r/l)^{0.8} + (z/l)^{1.3}} |P| \quad P < 0 \qquad (9)$$

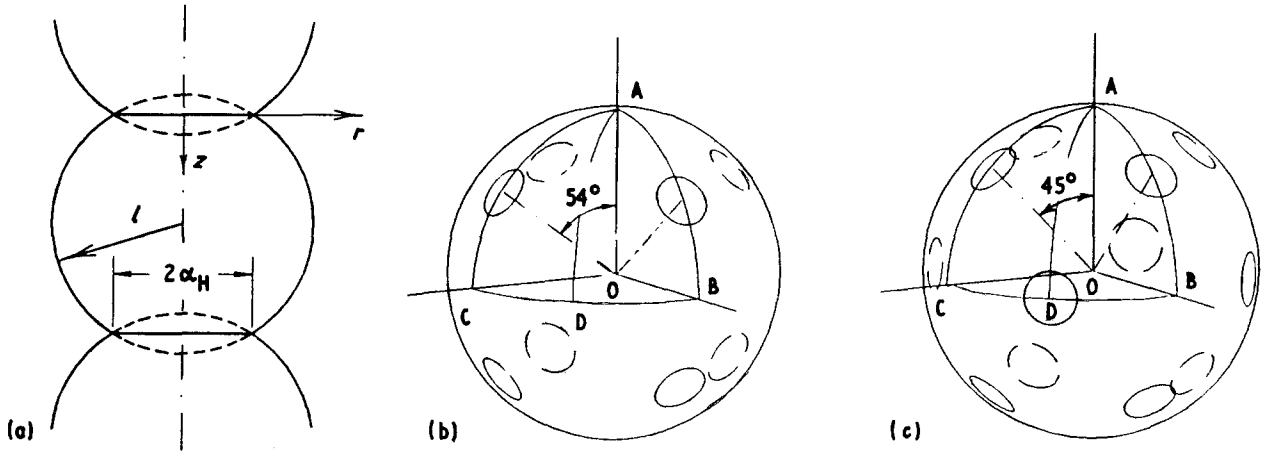

Figure 7 Schematic drawings of loading spherical nanoparticles by the closest neighbours in compressed nanopowders. (a) Two-contact loading. (b) Eight-contact loading corresponding to the b c c packing of nanoparticles in ensembles. Calculations have been carried out for the sphere element OABC, cut off from the sphere by symmetry planes. (c) Twelve-contact loading corresponding to the h c p packing of nanoparticles in ensembles. Calculations have been carried out for the same sphere element OABC.

TABLE I Hydrostatic stress at the centre of a loaded nanoparticle

	Number of contacts, Z					
	2		8		12	
α/l	P_m/G	P/G	P_m/G	P/G	P_m/G	P/G
0.05	7.6×10^{-5}	1.5×10^{-4}	3.2×10^{-4}	3.5×10^{-4}	4.5×10^{-4}	4.2×10^{-4}
0.1	6.0×10^{-4}	1.2×10^{-3}	2.5×10^{-3}	2.8×10^{-3}	3.7×10^{-3}	3.4×10^{-3}
0.15	2.0×10^{-3}	4.1×10^{-3}	8.6×10^{-3}	9.6×10^{-3}	1.3×10^{-2}	1.2×10^{-2}

The average external pressure, P, has been estimated as the superposition of two-contact loadings. From Fig. 7 it follows that $P = 4\cos54°P_{two}$ in the case of the eight-contact loading and $P = 4\cos45°P_{two}$ for the twelve-contact case.

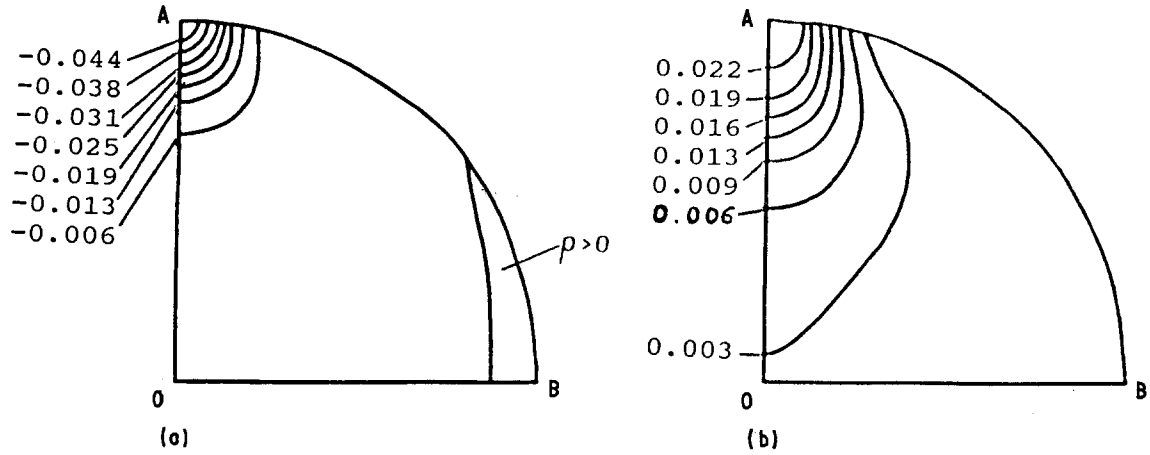

Figure 8 Stressed state in a spherical nanoparticle having two Hertzian contacts. (a) Hydrostatic stress. (b) Intensity of shear stresses. Data are expressed in terms of E (Young's modulus).

where z is the coordinate along the loading axis and r is the radial coordinate in a polar system with the origin coinciding with the contact centre. These equations agree within 30% with the numerical data.

4.2. An eight-contact model (Fig. 7b)

The eight-contact loading corresponds to the bcc packing of nanoparticles which is widespread in real powders [33]. The numerical results for the physically most peculiar cross-sections OAB and OAD (see Fig. 7) of a loaded nanoparticle are presented in Fig. 9. This figure shows the hydrostatic stress and the intensity of shear stresses over these cross-sections. As one may expect, the dilated volume is smaller than in the case of a two-contact model and corresponds to 2% of the total nanoparticle volume.

The superposition of dependencies, Equation 8 to obtain the hydrostatic stress or Equation 9 to obtain the intensity of tensile stresses, agrees for four pairs of contacts with the numerical results for the eight-contact problem within 30%.

The intensity of shear stresses in this loading geometry reveals maxima both under the Hertzian contacts and between them (see Fig. 9b, d).

4.3. A twelve-contact model (Fig. 7c)

The twelve-contact loading corresponds to the hcp packing of nanoparticles (the closest packing of rigid spheres). This type of packing is frequent in powders with a high green density (especially in dense clusters of nanoparticles).

Fig. 10 demonstrates the hydrostatic stress and the intensity of shear stresses for peculiar cross-sections OAB and OAD (see Fig. 7c). Except for being smoother, the maps of stresses principally resemble those for the eight-contact model. The fraction of dilated volume is negligibly small.

The numerical data in this case also lie within 30% of the values given by the two-contact equations (see Equations 8 and 9).

From Figs 8–10 one can see that the two-contact loading produces the most inhomogeneous distribution of hydrostatic and shear stresses. There are two scales of inhomogeneity in a loaded nanoparticle. The fine scale is determined by the contact radius, α_H, and the main scale by the intercontact distance which is of the order of l.

A larger number of contacts favours the hydrostaticity diminishing the intensity of shear stresses in the central regions of nanoparticles. Table I demonstrates this increase of hydrostatic stresses in the centre of a loaded nanoparticle, P_m, with the increase of the coordination number Z.

It follows from this table, that the hydrostatic stress in the centre of a nanoparticle tends to the value of external pressure as the coordination number, Z, becomes large, i.e. the stresses in nanoparticles become primarily hydrostatic. The deviations from hydrostaticity may be most clearly seen in the case of two contacts. In fact, a rather extended region with positive dilatation is formed in the case of the two-contact loading of nanoparticles. The dimensions of this region essentially decrease with the coordination number Z increasing.

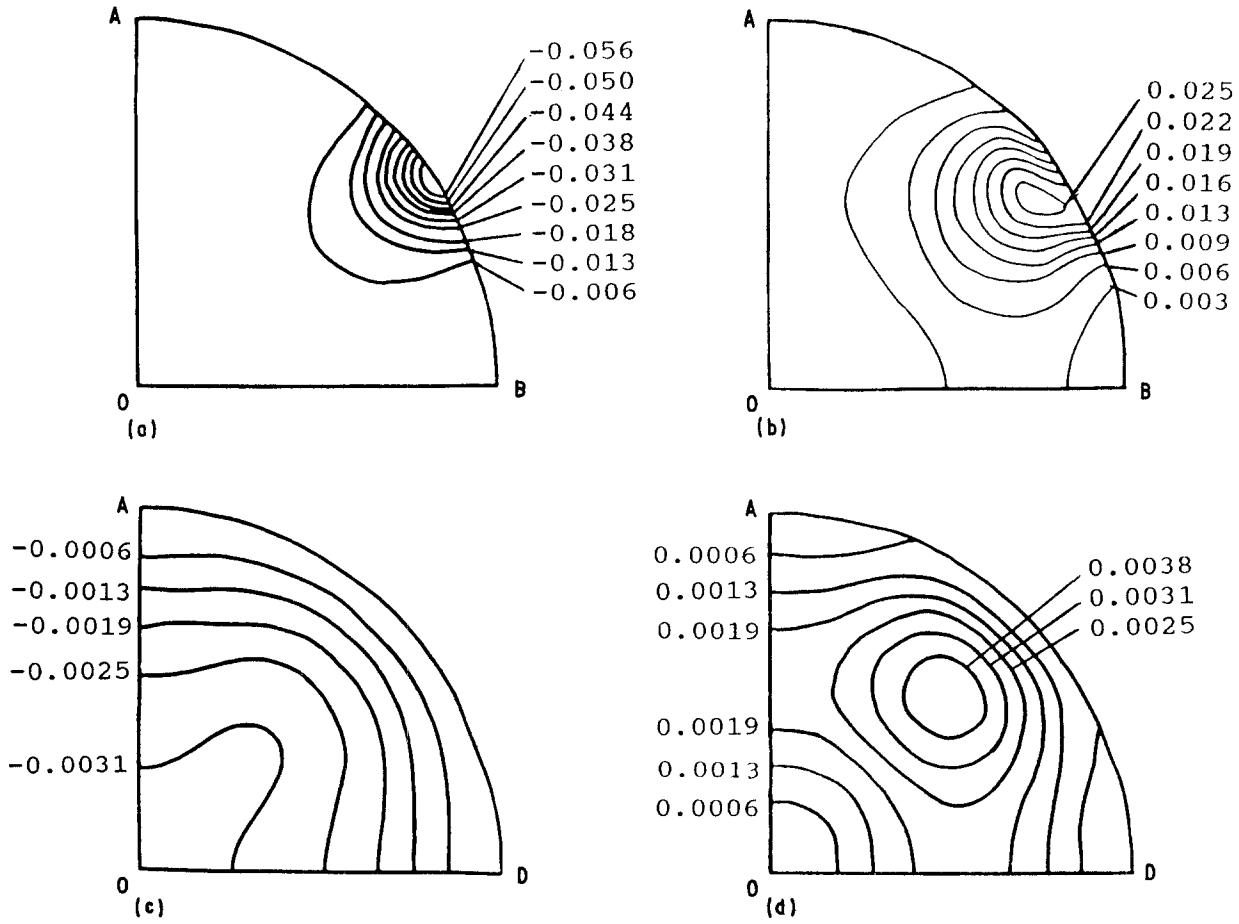

Figure 9 Stressed state in a spherical nanoparticle having eight Hertzian contacts. (a) Hydrostatic stress in OAB cross-section. (b) Intensity of shear stresses in OAB cross-section. (c) Hydrostatic stress in OAD cross-section. (d) Intensity of shear stresses in OAD cross-section. Data are given in terms of E (Young's modulus).

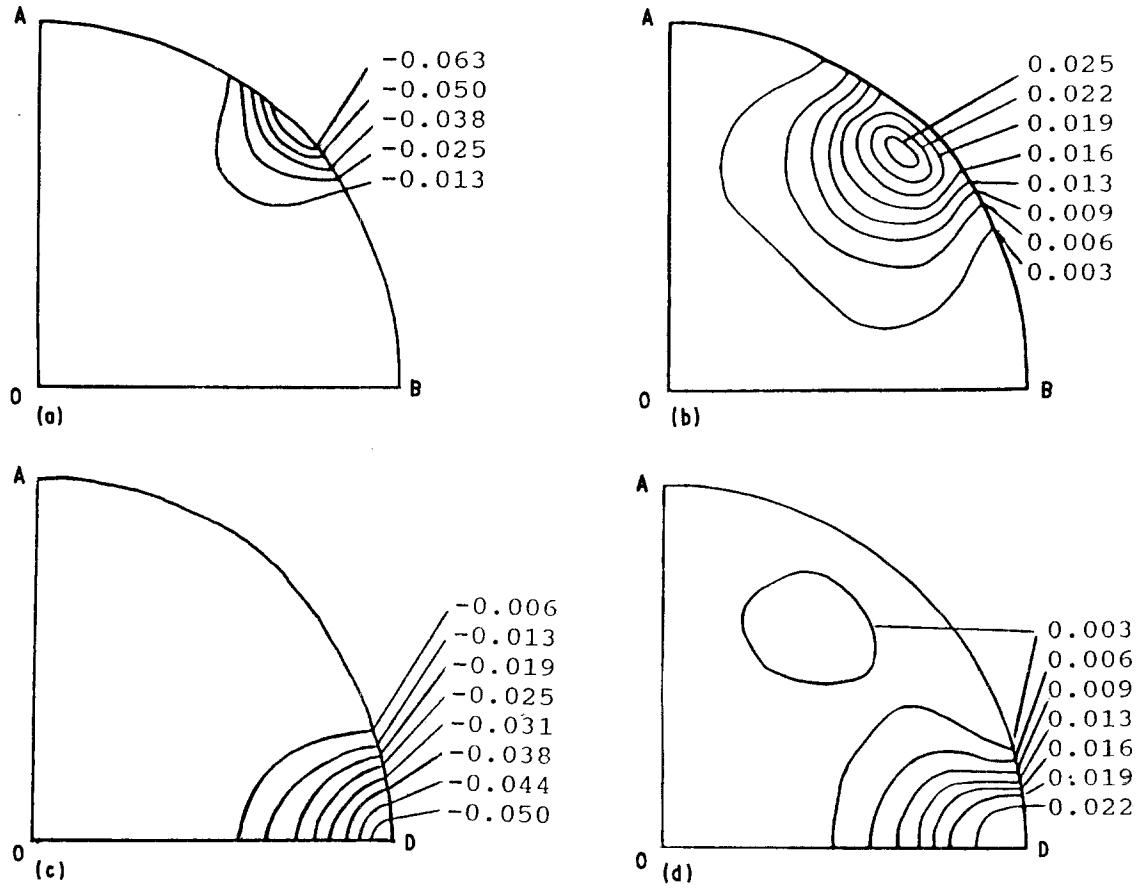

Figure 10 Stressed state in a spherical nanoparticle having twelve Hertzian contacts. (a) Hydrostatic stress in OAB cross-section. (b) Intensity of shear stresses in OAB cross-section. (c) Hydrostatic stress in OAD cross-section. (d) Intensity of shear stresses in OAD cross-section. Data are given in terms of E (Young's modulus).

It is peculiar that the volume of the dilated region is practically independent of the external load and is mainly determined by the coordination number, Z. Thus, the segregation processes should first develop in nanopowders with low green density *ceteris paribus*.

All these results are valid if the interparticle sliding processes in the nanopowders under compaction are completely finished and a perfect packing of nanoparticles is achieved (i.e. the contact shear loading is non-essential).

The influence of diffusion processes on the contact geometry has been neglected here. In fact, this may be done either under the conditions of low homologous temperatures or when the local stresses are not high enough to form the interstitials [19] (see Section 6).

If the diffusion neck develops, very high local stresses must appear near it [34]. These stresses $\sigma_{loc} \sim \bar{\gamma}/h$ (where h is the radius of the diffusion neck, see Fig. 6a) rarely exceed 1 GPa. However, if one takes into account the small value of radius h ($h \sim \alpha_H^2/l \approx 1$ nm) for typical nanoparticles, then according to the Saint-Venant principle [10] these stresses should rapidly fall at distances of the order of several h. This conclusion coincides with the results reported previously [34].

Thus, in real loaded nanoparticles, one can discern three types of stress inhomogeneities according to their size:

1. inhomogeneity decreasing at distances proportional to the diffusion neck radius, h;
2. inhomogeneity with the scale of the order of the Hertzian contact radius, α_H, see above;
3. inhomogeneity with the typical size proportional to the nanoparticle size, l.

In accord with the Saint-Venant principle, the small deviations from the spherical shape (asperity, facets, impurities, etc.) should not drastically influence the stress fields in the main part of the nanoparticle volume (elastic fields are disturbed only in the vicinity of imperfections). Nevertheless, when the scale of asperity approaches the contact radius α_H, the stress field should be seriously disturbed over the whole nanoparticle volume.

The study of the stressed state of nanoparticles in the ensembles exposed to high external pressures presents a difficult problem. The field of theoretical consideration is substantially narrowed, because at such pressures the linear theory of elasticity fails in the main part of the nanoparticle volume. Even at $\alpha_H = 0.15\,l$ the deformation, ε, right under the Hertzian contact which is about 0.1, is close to the margin of validity of the linear theory of elasticity.

5. Plastic relaxation of contact stresses

The maximum shear stress near the contact area may be approximately described by formula $\tau \sim [(1 - 2\nu)/2(1 - \nu)]\sigma_{max}$ [14]. The intensity of the contact stress fields described above is rather large at the initial stages of nanopowder compaction (e.g. at $P \sim 0.1$–1 GPa the contact local stress, σ_{loc}, may be as large as 10 GPa, which is close to the theoretical strength). If external pressure exceeds a certain value, P, the near-contact shear stress, τ, makes the lattice dislocations formed by interface dislocations (see Fig. 11) overcome the potential barrier and leave the interface. The Orowan criterion ($\tau_{loc} > 2\,G\boldsymbol{b}/D$‡, where τ_{loc} is the local shear stress) [35] should be fulfilled so that the dislocation segment of length, D, could spread into the nanoparticle volume (Fig. 11). This criterion implies that the external pressure, P, should obey the following condition

$$P > P^{(1)}(l) \sim \theta_4 G(\boldsymbol{b}/D)^3 \qquad (10)$$

where $\theta_4 \approx 10^1$. The substitution of typical values for the parameters entering this expression gives $P^{(1)} \approx 1$ GPa.

In the case of nanopowder mixtures, the formation and development of the dislocation half-loops occurs in the field of their image forces $\sim \theta'(G^{(2)} - G^{(1)})\boldsymbol{b}/(G^{(2)} + G^{(1)})z$, where $\theta' \approx 10^{-1}$ and z is the maximum distance from the half-loop to the contact (Fig. 12). If the shear modulus of the nanoparticle $G^{(1)}$ is less than that of its neighbour, $G^{(2)}$, these forces stimulate the spread of a half-loop into the nanoparticle volume, otherwise they prevent half-loops from spreading.

When the segments of the spreading loop with the screw components of the Burgers vector have low mobility as for some b c c metals, or, when the loops from neighbouring contacts block their lateral spread, the loop of interest may be treated as a narrow dipole (Fig. 12a).

This model allows a simple estimation of the irreversible spread of such a dipole. Really, under the action of contact stresses, this dipole may pass through the nanoparticle volume or react with other segments which results in the formation of the sessile dislocation configurations, or it may be captured by plane defects (twins, stacking faults, etc.) which are responsible for the irreversibility of plastic processes. Using Equation 9 and the approach proposed in [19], one may obtain the following relation for the characteristic pressure corresponding to the beginning of the plastic deformation of nanoparticles due to the irreversible spread of the dislocation dipoles

$$P^{(2)}(l) \sim \theta_5 G(\boldsymbol{b}/l)^{1/2} \qquad (11)$$

where $\theta_5 \sim 1$–10. At large l ($l \gg l^*$, see [31]) the nanoparticles possess their own mobile dislocations and this estimate should not be used. It is interesting to note that Equation 11 yields the same thresholds $P^{(2)}(l)$ for ceramic and metallic nanoparticles, because the shear moduli of these materials do not differ significantly. This approach may, particularly, explain the disappointing results on the compressibility of ceramic and metal nanopowders reported previously [36, 37].

On the other hand, if the Peierls barrier, σ_p, is very high (criterion $l > l^*$ is almost always fulfilled), the generated dipoles may be retained in the nanoparticle

‡ Other theories [10] predict a slightly smaller value of the factor entering this expression.

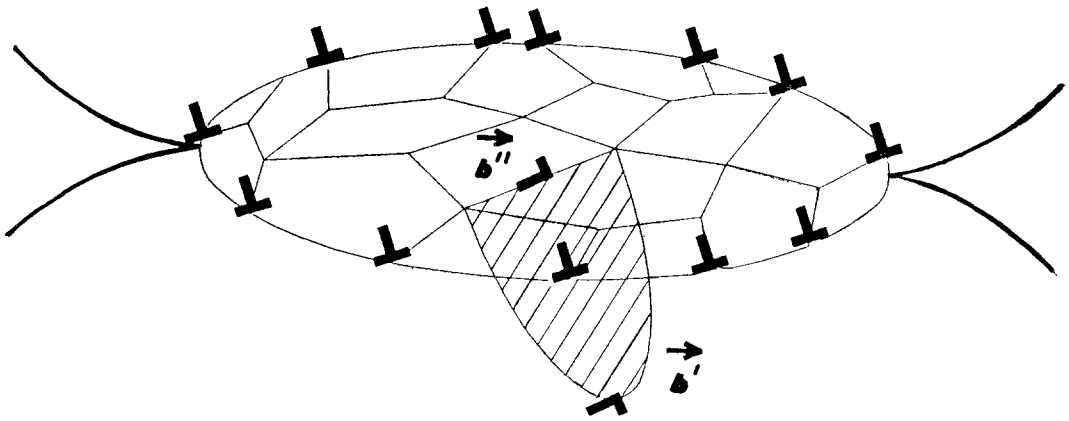

Figure 11 Spread of a segment of an interface dislocation caused by contact stresses and the formation of partial dislocation with the Burgers vector $\boldsymbol{b}'$.

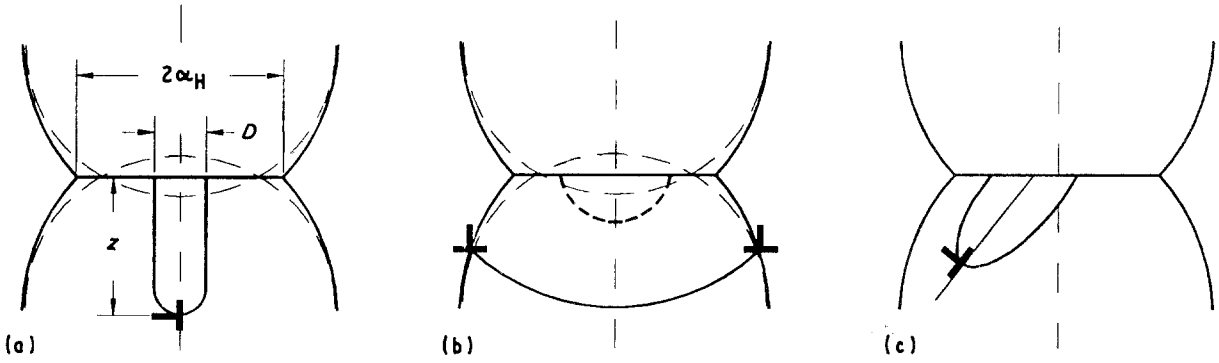

Figure 12 Models of the generation of dislocation half-loop from the Hertzian contact. (a) Dislocation dipole spreading downwards in the case when dipole lateral segments with screw components of the Burgers vector exhibit low mobility. (b, c) Front and side views of the broad half-loop in the case when dipole lateral segments with screw components of the Burgers vector have high mobility.

volume without any assistance of other defects. Under the narrow-dipole approximation this may occur if the following inequality is valid:

$$\sigma_p > \theta_6 G\boldsymbol{b}/D \qquad (12)$$

where $\theta_6 \sim 10^{-1}$. The typical value of parameter $\boldsymbol{b}/D$ in this case is about 10^{-1} and Equation 12 should hold for nanoparticles of germanium, silicon and for most ceramic materials (the latter have the critical length of dislocation stability $l^* \sim 1$ nm). Thus, the plastic deformation in these materials should always be irreversible.

When the screw components of the dislocation have high mobility (e.g. for fcc metals) the half-loop may not be approximated by a narrow dipole (Fig. 12b). In this case the distance between the points of intersections of the half-loop with the nanoparticle surface is comparable with radius l and depends on the external pressure P. Elastic image forces are more intense than in the previous model (because the dislocation line is effectively closer to the nanoparticle surface), so they can overcome the dislocation linear tension and become the main factor in the irreversible spread of dislocations. One may obtain the characteristic pressure corresponding to the initiation of the irreversible plastic deformation of a nanoparticle [19]

$$P'^{(2)}(l) \sim \theta_7 G\boldsymbol{b}/l \qquad (13)$$

where $\theta_7 \sim 10^{-1}$–10^{-2}. One should note that for fcc metals the height of the Peierls barrier, σ_p, cannot influence the estimate because this stress in such a case is rather low [10].

On the one hand, the spread of partial dislocations is facilitated by the small value of the Burgers vector; on the other hand, it is hindered due to the connection of the stacking fault with the partials. Such stacking faults of the "deformation" origin may be left in the nanoparticle volume after unloading a nanopowder specimen. Perhaps, it is these defects that have been observed in as-compacted nanopowders [38].

It follows from the considerations presented above, that the nanopowders consisting of the particles whose dimensions l are less than the critical length of the dislocation stability l^* [31] may reveal under compaction the threshold dependence of densification on the applied pressure, P. (Probably, such a threshold has been observed by Trusov *et al.* [39].) The threshold value may be estimated as $\theta G(\boldsymbol{b}/l)^m$, where θ and m are specific to the material. The threshold value for the ensemble of nanoparticles with sizes $l < 10^2$ nm may considerably exceed the typical pressure needed to compact coarse powders, which is several hundred megapascals.

One should bear in mind that the obtained threshold values of pressure should be considered only as the order-of-magnitude estimates, because most expressions contain poorly defined factors, θ. In addition, the densification–pressure diagrams may be smeared by an unavoidable dispersion in nanoparticle sizes, the irregular stacking of nanopowder particles and the

non-identity of contacts. The temperature increase should have the same effect, and it should diminish the values of $P^{(1)}$, $P^{(2)}$ and $P'^{(2)}$.

The diffusion necks may influence plastic processes in coarse powders [34, 40] bringing about the appearance of the sintering rosettes resulting from the redistribution of dislocations near the neck. The generation of dislocations by diffusion necks (self-indentation [40]) is, of course, hardly probable, because the diffusion neck stresses, which decay rapidly in nanoparticle volume (the characteristic decay range is about a few nanometres, see Section 4), do not provide any mechanism-stabilizing glissile dislocations. However, the stresses provided by the surface tension and existing near the diffusion neck may appreciably effect the mass-transfer processes at the periphery of contact interfaces (see the next section).

6. Diffusion near contact interfaces

Nanopowders are in many aspects unique objects, particularly in the sense that in the pre-threshold region of pressures (see Section 4) one may excite very high local stresses over the whole nanopowder volume, which persist for considerable time periods. The plastic relaxation of stresses makes such a situation practically unreproducible in other objects.

This section is devoted to the analysis of specific features of diffusion in nanopowders when the external pressure, P, does not exceed the threshold value corresponding to the origination of irreversible plastic processes in nanoparticles. The present consideration touches only upon the temperature region $T \sim 0.1$–0.3 T_m (where T_m is the melting temperature), where exaggerated recrystallization and the processes of normal diffusion are weakly pronounced.

At the initial stage of deformation when the nanoparticle shape is close to spherical, the gradients of stresses in the contact region $\nabla p \sim p/\alpha_H$ (where $p \sim P(1/\alpha_H)^2$ is the local hydrostatic stress) differ noticeably from those in the nanoparticle volume $\nabla p \sim P/l$. The former are easily seen to be greater by an order of magnitude. In addition, the enthalpy of the defect formation changes by $p\Delta V_F$ (where ΔV_F is the activation volume of defect formation). Owing to this fact, the probability of the formation of a vacancy in the contact region decreases, while the probability of forming an interstitial grows. Each diffusion mechanism acts during its typical time period, τ. These typical periods may be estimated if one takes the gradients of contact stresses to be effective up to distances $r \sim \alpha_H$ from the contact (Fig. 13).

Under the action of the contact stress gradients, ∇P, the impurity atoms may leave the contact interface and diffuse towards the nanoparticle-free surface. One may obtain the corresponding estimate [19]

$$\tau_{im}^{(c)} \sim \frac{kT}{G\Delta V_F^{(c)}} \frac{l^2}{D_{im}^{(c)}} \left(\frac{P}{G}\right)^{1/3} \tag{14}$$

where superscript c indicates values relevant to the contact interface, and D_{im} is the diffusion coefficient of the second component.

If, initially, the second component is uniformly dissolved in the nanoparticle volume, then under the action of the volume gradients, ∇p, resulting in the stress-stimulated diffusion, the homogeneity of the composition is broken in the time given by expression

$$\tau_{im}^{(v)} \sim \frac{kT}{G\Delta V_F^{(v)}} \frac{l^2}{D_{im}^{(v)}} \left(\frac{G}{P}\right)^{1/3} \tag{15}$$

where superscript v denotes the diffusion processes in the volume. From this relationship it follows that the higher the external pressure and the smaller the particle size, the greater this inhomogeneity in the distribution of the second component. The allowance for the dependence of $D_{im}^{(v)}$ on the local stresses will produce a more involved dependence of $\tau_{im}^{(v)}$ on P.

One may realize that the concentration of the second component with $\Delta V_F < 0$ (i.e. vacancies, substitutional atoms with a diameter less than the dimensions of the lattice atoms) may locally increase in the vicinity of the contact area, while the second component with $\Delta V_F > 0$ (i.e. the interstitials and the substitutional atoms with large radii) should evidently diffuse towards the nanoparticle-free surface.

The Hertzian stresses may stimulate the self-diffusion processes in one-component nanoparticles similarly to the stress-stimulated diffusion of adsorbed and dissolved atoms in two-component nanoparticles. In the present case an appreciable mass transfer brings about an irreversible nanoparticle deformation and, hence, the relaxation of contact stresses. Possible mechanisms of self-diffusion are considered below.

For the contact–interface stress-stimulated self-diffusion the material is transferred from the centre of the

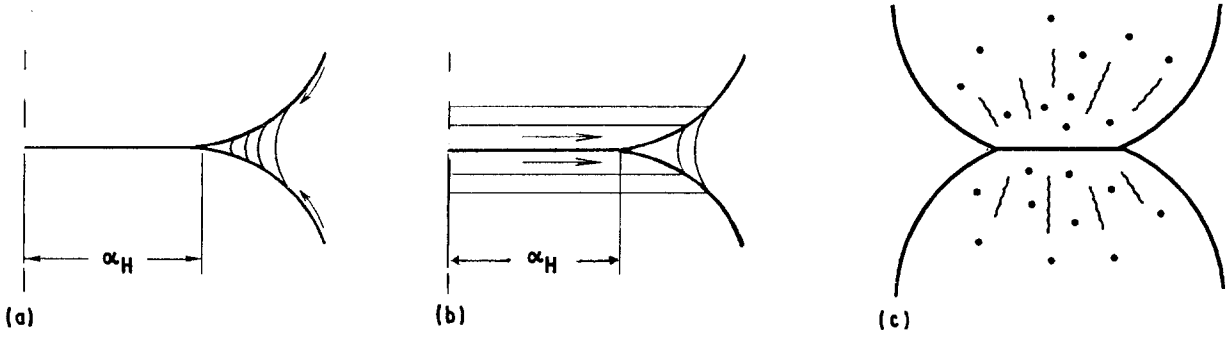

Figure 13 Diffusion mechanisms providing stress relaxation in interface contacts. (a) Interface (boundary) diffusion. (b) Surface diffusion. (c) Volume diffusion via an interstitial mechanism (wavy lines represent crowdions).

contact towards its periphery in a thin layer of width, a (Fig. 13a). Assuming the contact stresses to fall at a distance of the order of the contact radius, one can obtain [19]

$$\dot{\varepsilon}_c \sim \frac{G\Delta V_F^{(c)}}{kT} \frac{D^{(c)}a}{l^3} \left(\frac{P}{G}\right)^{1/3} \quad (16)$$

The deformation rate for the process of the surface stress-stimulated self-diffusion may be estimated using the assumption, that under the action of the "surface" hydrostatic local stress, p', the atoms drift over the surface layer of width, a', into the neck region (see Fig. 13b). The corresponding expression has the following form [19]:

$$\dot{\varepsilon}_s \sim \frac{G\Delta V_F^{(s)}}{kT} \frac{D^{(s)}a'}{l^3} \left(\frac{P}{G}\right)^{1/3} \quad (17)$$

where superscript s denotes the phenomena at the nanoparticle surface.

Under certain conditions, the stress-stimulated self-diffusion proceeding via the interstitial mechanism (Fig. 13c) may turn out to be the main channel of the relaxation of elastic stresses. It is highly probable that the crowdions and interstitials are formed in the contact region where the stress concentration is maximum (e.g. near the vertices of the nanoparticle habitus which are set against the facet of the neighbouring nanoparticle, or near the facet steps, see Section 3).

The enthalpy of the formation of interstitials and crowdions under the action of the contact pressure, p, considerably decreases by the value of $-p\Delta V_F^* + \Delta SkT$ [41], where ΔV_F^* is the activation volume of forming an interstitial, ΔS is the relative change in the entropy associated with forming an interstitial or a vacancy. In contrast to interstitials, the formation of vacancies is suppressed, the concentration of thermodynamically equilibrium vacancies being decreased by a factor of $\exp(-p|\Delta V_F|)$. In this case, the preferable interstitial formation will determine the self-diffusion processes via the interstitial mechanism. The proper deformation rate has the following form [19]:

$$\dot{\varepsilon}_v \sim \frac{G\Delta V_F^*}{kT} \frac{D_i^{(v)}}{l^2} \left(\frac{P}{G}\right)^{2/3} \quad (18)$$

where $D_i^{(v)}$ is the coefficient of the volume self-diffusion via the interstitial mechanism.

The heterogenization in nanoparticles with the initially uniform distribution of the second component, accounted for by the diffusion caused by the Hertzian stresses, has been considered by Tanakov *et al.* [42]. It has been shown that in the first moments the concentration of the second component along the loading axis (see Fig. 14) changes non-monotonically. After a certain delay the second component acquires a monotonic spatial distribution in the vicinity of the Hertzian contact.

The surface tension playing an important role in the classical theory of sintering has been ignored in Equations 16–18. The characteristic pressure above which the Hertzian stresses prevail over the surface tension in the mass-transfer processes in nanoparticles may be

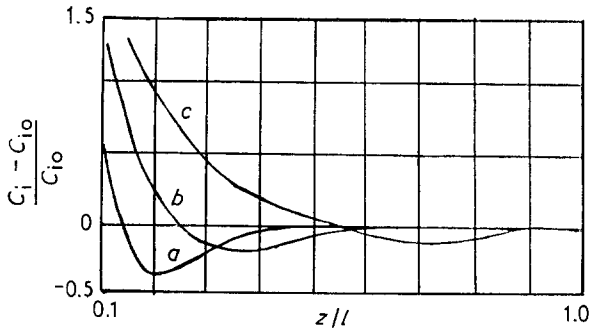

Figure 14 Relative variation of second-component concentration $(c_{i0} - c_0)/c_{i0}$ in nanoparticles with depth at three time moments. The dependence presented refers to the case of the second-component atoms (or defects) with a negative activation volume, ΔV_F.

estimated as

$$P' = \theta_8 \left(\frac{\bar{\gamma}}{\gamma_d}\right)^2 \frac{\bar{\gamma}}{l} \quad (19)$$

where the numerical factor $\theta_8 \approx 1$. The substitution of the proper parameters gives the value $P' \approx 0.1$–1 GPa. Thus, for higher external pressures, surface tension effects may be neglected.

As shown in Section 5, the nanoparticle plastic deformation due to the exit of interface dislocations into the nanoparticle volume may take part in relaxation phenomena and compete with diffusion. The rate of plastic deformation corresponding to this process may be approximately written as [19]

$$\dot{\varepsilon}_d \sim \frac{bv}{l\mathscr{D}} \left(\frac{P}{G}\right)^{2/3} \quad (20)$$

where v is the velocity of dislocation translation.

The dislocation channel of the contact stress relaxation is efficient, as long as the external pressure exceeds the threshold value, $P^{(2)}(l)$, corresponding to the irreversible development of plastic deformation (see Section 5). In this case the rate of plastic deformation exceeds the rate of deformation provided by diffusion mechanisms (see Equations 16–18). Therefore, the condition which determines the possibility of the dislocation channel dominating over the diffusion one, may be written as the condition imposed on the velocity of the translation of dislocation in loaded nanoparticles

$$v \gg \begin{cases} \dfrac{G\Delta V_F^{(c)}}{kT} \dfrac{D^{(c)}a}{l^2} \dfrac{\mathscr{D}}{b} \left(\dfrac{G}{P}\right)^{1/3} \\ \dfrac{G\Delta V_F^{(s)}}{kT} \dfrac{D^{(s)}a'}{l^2} \dfrac{\mathscr{D}}{b} \left(\dfrac{G}{P}\right)^{1/3} \\ \dfrac{G\Delta V_F^*}{kT} \dfrac{D_i^{(v)}}{l} \dfrac{\mathscr{D}}{b} \left(\dfrac{G}{P}\right)^{1/3} \end{cases} \quad P > P^{(2)} \quad (21)$$

Hence, the high rates of loading and appreciable external pressures are required to ensure the effective relaxation of contact stresses in nanoparticle ensembles at the expense of plasticity.

The considered processes of the stress-stimulated diffusion of dissolved and adsorbed atoms in multicomponent nanoparticles may modify their physical

TABLE II Exponents characterizing mass-transfer kinetics in contacts

Diffusion mechanism	Surface tension		Hertzian stresses	
	n	m	n	m
Intercrystallite	6	4	6	3
Surface	3–7	2–4	5	3
Volume (Interstitial)	4–5	3	5	2

and mechanical properties. The inhomogeneous distribution of the second-component atoms over the nanoparticle volume may locally change the elastic moduli and the Peierls barrier height. In addition, a new phase may be formed in the regions of the maximum concentration of the second component. This phase may considerably retard the development of plastic deformation in nanoparticles and worsen the compaction conditions.

The lattice deformation of contacting nanoparticles may also lead to the dissolution of impurities, adsorbed by the surface of a nanoparticle, in the crystal lattice. The time required for this process may be estimated using Equation 15. On the one hand the dissolution of the impurity atoms hardens the nanoparticle material; on the other hand, it may clear up the nanoparticle surface from the impurities.

Substituting the typical values of parameters $T = 293$ K, $P \approx 10^{-1}$ GPa, $\alpha_H/l \approx 10^{-1}$, $D_{im}^{(c)} \sim 10^{-15}\,m^2\,s^{-1}$, $D_{im}^{(v)} \sim 10^{-17}\,m^2\,s^{-1}$, $\Delta V_F \sim 10^{-2}$–$10^{-1}a^3$ into Equations 14 and 15, one may show that the heterogenization in the contact interface and in the nanoparticle volume can occur in times $\sim 10^{-2}$–10^{2} s.

For one-component nanoparticles, the estimates (Equations 16–18) for the rate of contact stress relaxation may be rewritten in the form of the well-known formula of the contact radius kinetics $(\alpha/l)^n = Cl^{-m_t}$ [43], where n, m, C are the constants characterizing the particular mechanism of mass-transfer, and t the duration of isothermal sintering. The computed values of exponents n and m for the surface tension [43] and for the Hertzian contact stresses are given in Table II. It is clearly seen from this table, that the external hydrostatic pressure applied to nanopowders changes the kinetics of the low-temperature sintering. One should note that for the nanoparticles with the size l exceeding the characteristic length l^* [31] of the dislocation stability, the results for Hertzian contacts lose their validity.

References

1. H. GLEITER and B. CHALMERS, *Prog. Mater. Sci.* **16** (1972) 1.
2. B. S. BOCKSTEIN, Ch. V. KOPETSKII and L. S. SCHWINDLERMAN, "Thermodynamics and Kinetics of Grain Boundaries in Metals" (Metallurgia, Moscow, 1986) in Russian, p. 233.
3. V. M. IEVLEV, L. I. TRUSOV and V. A. KHOLMYANSKII, "Structural Transformations in Thin Films" (Metallurgia, Moscow, 1982) in Russian, p. 248.
4. I. D. MOROKHOV, L. I. TRUSOV and S. P. CHIZHIK, "Highly Dispersed Metallic Media" (Atomizdat, Moscow, 1977) in Russian, p. 264.
5. R. ROMANOWSKY, "Highly Dispersed Metals" (Wiley, New York, 1987).
6. Yu. I. PETROV, "Clusters and Small Particles" (Nauka, Moscow, 1986) in Russian, p. 366.
7. K. L. JOHNSON, K. KENDALL and A. D. ROBERTS, *Proc. R. Soc. A (Lond.)* **324** (1971) 301.
8. K. KENDALL, N. McN. ALFORD and J. D. BIRCHALL, *ibid.* **412** (1987) 260.
9. L. I. TRUSOV, V. I. NOVIKOV and V. N. LAPOVOK, *Sci. Sintering* (1991) **23** (1991) 63.
10. J. P. HIRTH and J. LOTHE, "Theory of Dislocations" (McGraw-Hill, New York, 1983).
11. V. G. GRYAZNOV and L. I. TRUSOV, *Phys. Met. USSR* **8** (1986) 100.
12. E. N. YAKOVLEV, G. M. GRYAZNOV, V. I. SERBIN, V. N. LAPOVOK, L. I. TRUSOV, N. B. KUKHAR, V. Ya. GANELIN, E. V. KAPITANOV and V. B. BEGOULEV, *Phys. Chem. Mech. Surf.* **2** (1984) 1199.
13. V. I. NOVIKOV, V. Ya. GANELIN, L. I. TRUSOV, V. N. LAPOVOK, I. A. SHUTOV, E. N. YAKOVLEV, L. G. KHVOSTANTSEV, T. P. GELEISHVILI and N. D. KVATAYA, *Phys. Metals (USSR)* **8** (1986) 111, in Russian.
14. A. I. LURIE, "Theory of Elasticity" (Nauka, Moscow, 1970) in Russian, p. 939.
15. G. KARAMI, in "Lecture Notes in Engineering", Vol. 51, edited by C. A. Brebbia and S. A. Orszag (Springer, Berlin, 1989), p. 243.
16. L. R. WALLENBERG and J.-O. BOVIN, *Naturwiss.* **72** (1985) 539.
17. S. IIJIMA, *J. Elect. Microscopy* **34** (1985) 249.
18. L. D. MARKS, in "Structure and Dynamics of Surfaces", Vol. 1, edited by W. Schommers and P. von Blanckenhagen (Springer, Berlin, 1986) p. 71.
19. V. G. GRYAZNOV, M. Yu. TANAKOV, L. I. TRUSOV and V. A. SOLOV'EV, to be published.
20. V. I. VLADIMIROV and A. E. ROMANOV, "Disclinations in Crystals" (Nauka, Leningrad, 1986) in Russian, p. 223.
21. I. HANSSON and A. THOLEN, *Phil. Mag. A* **37** (1978) 535.
22. A. R. THOLEN, *Acta Metall.* **27** (1979) 1765.
23. H. ICHINOSE and Y. ISHIDA, *Phil. Mag. A* **60** (1989) 555.
24. A. P. SUTTON and V. VITEK, *Phil. Trans. R. Soc. A (Lond.)* **309** (1983) 1.
25. W. WUNDERLICH, Y. ISHIDA and R. MAURER, *Scripta Metall. Mater.* **24** (1990) 403.
26. A. R. THOLEN, *Z. Phys. D* **12** (1989) 123.
27. M. D. BENTZON, A. KARLEN and A. R. THOLEN, *Coll. Phys.* **51** (1990) C1-89.
28. K. JOHNSON, "Contact Mechanics" (Cambridge University Press, Cambridge, 1985), p. 452.
29. M. Yu. TANAKOV, L. I. TRUSOV, M. V. BELYI, V. E. BULGAKOV, and V. G. GRYAZNOV, *J. Phys. D.* (1992) to be published.
30. M. F. ASHBY, *Prog. Mater. Sci.* **25** (1980) 1.
31. V. G. GRYAZNOV, A. M. KAPRELOV and A. E. ROMANOV, *Scripta Metall.* **23** (1989) 1443.
32. I. C. NOYAN, *Phil. Mag. A* **57** (1988) 127.
33. V. V. SKOROKHOD and S. M. SOLONIN, "Physico-Metallurgical Foundations of Powder Sintering" (Naukova Dumka, Kiev, 1984) in Russian, p. 159.
34. W. SCHATT, E. FRIEDRICH and D. JOENSSON, *Acta Metall.* **31** (1983) 121.
35. J. FRIEDEL, "Dislocations" (Pergamon Press, London, 1964), p. 491.
36. R. A. ANDRIEVSKII, *Powd. Met. (USSR)* (8) (1988) 40, in Russian; English translation: *Sov. Powder. Metall. Met. Ceram. (USA)* **28** (1988) 627.
37. *Idem*, "Horizons of Powder Metallurgy" (Verlag Schmidt, Freiberg, 1986) p. 987.
38. L. I. TRUSOV, V. I. NOVIKOV, I. P. ARSENT'EVA, S. V. SVIRIDA, V. G. GRYAZNOV, V. N. LAPOVOK and A. N. SEMENIKHIN, *Izv. AN USSR* **50** (1986) 1593, in Russian; English translation: *Bull. Acad. Sci. USSR, Phys. Ser. (USA)* **50** (1986) 130.
39. L. I. TRUSOV, P. V. VLASOV, I. G. NAVMENKO, S. Yu. SOROKIN, V. A. SIDOROV, V. I. NOVIKOV, L. G.

KHVOSTANTSEV and O. M. GVOZDETSKII, in "Growth and Structure of Thin Films", edited by V. M. Ievlev (Voronezh Polytechnic Institute, 1990) in Russian, p. 55.
40. Ya. E. GEGUZIN, "Physics of Sintering" (Nauka, Moscow, 1984) in Russian, p. 309.
41. V. L. INDENBOM, *J. Exp. Theor. Phys. Lett. (USSR)* **12** (1970) 526, in Russian; English translation: *JETP Lett.* **12** (1970) 369.
42. M. Yu. TANAKOV, B. Ya. LJUBOV and L. I. TRUSOV, *Scripta Metall. Mater.* **25** (1991) 413.
43. H. E. EXNER and E. ARZT, in "Physical Metallurgy", Vol. 2, edited by R. W. Cahn and P. H. Haasen (North-Holland, Amsterdam, 1983).

Received 29 April
and accepted 2 August 1991